Spin Coating Photoactive Photosystem I−PEDOT:PSS Composite Films

Marc A. Nabhan, Carlos A. Silvera Batista, David E. Cliffel, and G. Kane Jennings*

Cite This: https://doi.org/10.1021/acsapm.2c02126

Read Online

ACCESS | Metrics & More | Article Recommendations | SI Supporting Information

ABSTRACT: Photosystem I (PSI), a naturally abundant multi-subunit protein complex known for its ability to harvest solar energy and transform it into chemical energy in photosynthesis, is mixed with an intrinsically conducting polymer (ICP) poly(3,4-ethylenedioxythiophene):polystyrenesulfonate (PEDOT:PSS) to deposit well-mixed thin films via spin coating from aqueous solution. This process enables uniform, reproducible, and rapid film formation in which the composition and thickness of composite films can be readily tuned up to a few hundred nanometers. We assess the size distributions of the system in solution as well as the composition, thickness, conductivity, scalability, and photoactivity of the resulting biohybrid PSI−polymer films. The combination of the protein and ICP yields

increased photocurrents and turnover numbers when compared to single-component films of the protein or ICP alone to reveal a synergistic combination of film components. Based on photocurrents and turnover numbers, the efficiency of integrating the protein with the polymer is highest at low PSI loadings where protein−polymer interactions are maximized.

KEYWORDS: biohybrid, photoactive thin films, spin coating, photosystem I, PEDOT:PSS, solar-energy conversion, composite films, photoelectrochemical devices
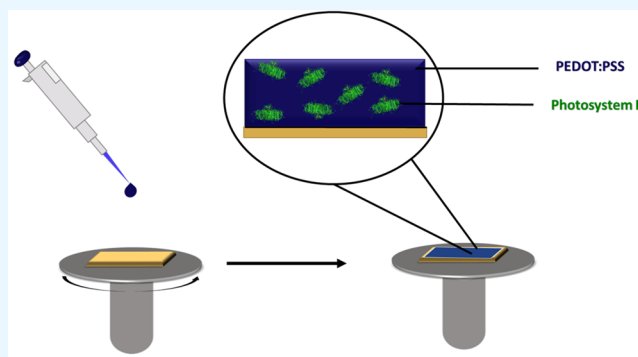
INTRODUCTION

Nature utilizes the sun through photosynthetic organisms that harvest solar energy and transform CO_2 into O_2 and carbohydrates through evolutionarily adapted protein complexes.[1] Photosystem I (PSI) is one such protein complex within the thylakoid membranes of chloroplasts. As a photoactive protein with nearly perfect quantum yield, PSI excels in absorbing photons and using their energy to translocate electrons from a chlorophyll *a* dimer, P_{700}, to P_{700}^* that readily donates an electron through a series of cofactors to an iron−sulfur complex known as F_B.[2] Through this process, PSI produces the greatest reducing potential in nature (−580 mV vs SHE at the F_B site) with a redox potential of 1.1 V across the protein complex and an electron transfer turnover rate of 50 e^- s^{-1} PSI^{-1} *in vivo*.[1,3,4]

PSI's vast availability, ease of extraction, compatibility with multiple organic compounds, and aptness to genetic engineering have all contributed to the surging interest in integrating this protein into a variety of energy conversion technologies in both wet and dry systems.[5] In these systems, PSI is often incorporated with other materials such as conducting polymers to facilitate electron transfer and elevate performance of the biohybrid film. Our aim in this study is to develop a rapid and straightforward process to prepare well-mixed PSI-conducting polymer composite films and to investigate the effect of PSI loading on photoelectrochemical properties. To be compatible with PSI, an interfacing material must maintain the stability and biofunctionality of the protein complex. Finding an appropriate PSI-conducting polymer mixture has far-reaching effects on the resulting biohybrid devices, and many aspects of the synthetic material must be considered to yield a successful polymer−protein coupling. Some of the factors of the polymer to consider are its redox potential, aqueous-phase solubility, chemical structure and functional groups, the type and density of its surface charges, and its conformational flexibility.[6] Once compatibility between the polymer and PSI has been confirmed, a wet-based or a solid-state system can be explored by using the well-mixed system.

A variety of conducting polymers are manufactured at an industrial level and are suitable for photovoltaic applications. PEDOT:PSS particularly stands out within this group as the most popular commercial polymer used in thermoelectric devices and photovoltaic cells,[7] and it offers multiple

advantages to pair with PSI for the preparation of biohybrid films. First, this widely studied ICP is considered water-soluble due to the presence of the polyanion (PSS) and can be easily incorporated into aqueous solutions that we use to process PSI.[8] Second, PEDOT:PSS has a flexible positively charged PEDOT-rich inner core and a negatively charged PSS outer shell that could interact well with the amphipathic PSI protein inducing high likelihood for favorable electrostatic interactions.[9] Third, this p-doped polymer is a hole conductor with redox potential favorable to both P_{700} and F_B active sites of PSI.[10,11] Fourth, PEDOT:PSS assists in extracellular electron transfer when combined with the cyanobacterium Synechocystis sp, emphasizing the ability of PEDOT:PSS to accommodate certain biological organisms and to maximize electrocatalytic reactions within a photoactive film.[12] Lastly, our group has identified strong electrostatic interactions between PSI and PEDOT:PSS where the protein adsorbs rapidly and with ease at the polymer's interface, and vice versa, to enable layer-by-layer (LbL) assemblies.[13] This strong coupling of PSI with PEDOT:PSS at interfaces suggests that these interactions can be driven in solution to disperse the protein complex.

PSI films have been predominantly deposited via drop casting, a facile and simple deposition method that deposits all the solution-based protein into the film and conserves the activity of PSI.[14] However, drop casted films are nonuniform, and the layers produced can be spatially inconsistent. In particular, the coffee-ring effect is omnipresent in this technique, causing an increase in thickness at the film boundaries.[15] We and others have used self-assembly to produce PSI films that are generally limited to (sub)monolayer amounts.[16,17] As another form of self-assembly, the LbL deposition method used by Wolfe et al. has proven successful in depositing up to 9-layer pairs of PSI and PEDOT:PSS with highly reproducible thicknesses, high loadings of PSI, and improved electron collection rate when compared to drop casted films.[13] However, each layer pair requires a 45 min timespan for deposition, with the resulting 80 nm thick, 9-layer-pair film requiring several hours to prepare. In contrast, spin coating is done on the order of 1 min and results in much thicker films, retaining a higher total loading of material at the surface of the electrode, in a much shorter timespan.

We herein report mixing PSI and PEDOT:PSS in solution and then spin coating the combined matrix for the straightforward fabrication of conductive composite polymer—protein films. Spin coating excels where drop casting, layer-by-layer deposition, and self-assembly lag by promoting uniformity and allowing for a tunable control of film thickness from tens to several hundred nanometers, providing a reliable and rapid alternative for our applications of interest. Uniformity is important in thin-film formation so that the thin film in the device can operate similarly in the 2D plane with consistent conductivity, composition, and thickness. However, membrane proteins are difficult to spin coat from pure aqueous solutions, forming thin and nonuniform deposits, even on treated and highly functionalized surfaces, as shown in Figure S1, and they typically require stabilizing molecules or cross-linkers in solution.[18] To overcome these challenges, mixing the protein in a supporting medium with the aim to increase overall viscosity and improve component affinity to the substrate is a valid pursuit. Here, we have selected PEDOT:PSS, which we hypothesize would interact well with PSI, replace some of the interactions between the protein and

its surfactant (TX-100), and help the aqueous mixture to interact well with the substrate to prevent excessive spin-off. Others have examined PSI and PEDOT:PSS in layered devices but not in the mixed manner achieved here. For example, Kazemzadeh et al.[19] immobilized PSI in a solid-state photovoltaic cell by depositing a distinct layer of PEDOT:PSS followed by PSI. In their device fabrication, PSI and PEDOT:PSS were spin coated separately for less than 10 s, but the amount of PSI retained in the layered structure was not reported.

In this work, we spin coat composite PSI films for the first time, and we examine the effects of PSI loading in the film by mixing PEDOT:PSS and PSI in solution at different percentages ranging from 0 to 70 wt % PSI in the solute (PSI+PEDOT:PSS). These thin films are easily fabricated, retain the two key components, and are electrically conductive. We control the thickness and achieve uniformity for the spin coated films by exploring the different aspects that impact the well-mixed nature and topology of the films. By understanding interactions of PSI with PEDOT:PSS in solution, we can achieve conductive, well-mixed, and uniform films via spin coating.

■ MATERIALS AND METHODS

Materials. PSI was extracted from organic spinach purchased at a local grocery store. Triton X-100 surfactant, 1.1 wt % PEDOT:PSS in water (surfactant-free, high conductivity grade), (3-aminopropyl)-trimethoxysilane, and 2-aminoethanethiol (AET) were purchased from MilliporeSigma. Silicon (100) wafers were purchased from WRS materials. Chromium-coated tungsten rods were purchased from R.D. Mathis. Gold shot (99.99% purity) was obtained from J&J Materials. Spectrum Laboratories regenerated dialysis membrane tubing (6000 to 8000 Da MWCO) was obtained from Fisher Scientific.

PSI Extraction. PSI was extracted from spinach following steps described in a previous work.[17] In summary, spinach was deveined, macerated, filtered, and then centrifuged at 8000g. The supernatant was then stabilized with a surfactant (Triton X-100) before a second centrifugation at 20000g. The resulting solution was passed through a hydroxyapatite column as the last step in isolating PSI.

Preparation of Gold Substrates. The gold substrates were prepared following a previously described method where silicon wafers are rinsed with deionized water and ethanol and then dried in a nitrogen stream.[20] Chromium (100 Å) and gold (1250 Å) were evaporated onto the processed silicon wafers at a rate of 2 Å/s or less. The evaporation was performed in a diffusion pumped chamber at a base pressure of 4×10^{-6} Torr. The wafers were then cut into 1.5 cm × 2.5 cm samples after evaporation. Self-assembled monolayers (SAMs) on gold surfaces were prepared by submerging the gold substrate into a 1 mM ethanolic solution of 2-aminoethanethiol (AET) for ~1 h, followed by rinsing with ethanol and drying in a N_2 stream.

Preparation of Glass Substrates. Microscope slides were cleaned with water and ethanol, before soaking in a 70% v/v H_2SO_4 and 30% v/v H_2O_2 (piranha solution) for 30 min to hydroxylate the surface (*warning: the mixture reacts violently with organic matter—handle with extreme caution!*). After piranha treatment, glass substrates were rinsed with water (thoroughly), then ethanol, and finally toluene. The substrates were then immersed in a solution of 600 μL of (3-aminopropyl)trimethoxysilane and 30 mL of anhydrous toluene for 30 min to obtain an amine-terminated primer on the surface of the glass. Spin coating was then used to deposit films at different PSI−PEDOT:PSS ratios onto the amine-terminated surface.

Spin Coating. Gold electrodes were removed from the AET solution, rinsed in ethanol, and dried under a stream of nitrogen. Extracted PSI (stabilized by TX-100) and PEDOT:PSS stock solution were mixed at different weight proportions as shown in Table S1
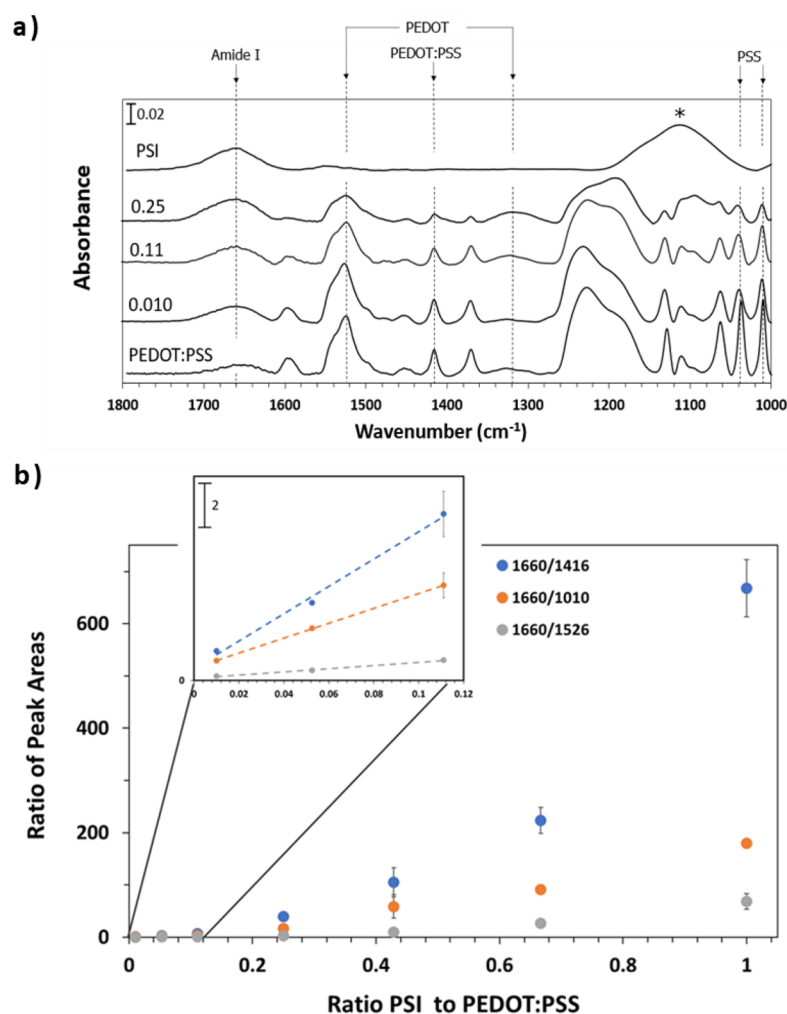
Figure 1. (a) FTIR/ATR spectroscopy of films with different ratios of PSI to PEDOT:PSS in solution revealing the retention of the spin coated material into the films, with the numbers above each graph representing the various ratios with spectra offset vertically for clarity. As the percent of PSI increases, the ratio of Amide I peak to all other PEDOT:PSS peaks increases. (∗) Peak due to TX-100. (b) Plot of the ratio of area under the curve at the amide I peak (1660 cm^{-1}) to the area under the curve of three PEDOT:PSS peaks (1010, 1416, and 1526 cm^{-1}) vs the ratio of PSI to PEDOT:PSS in solution. At a given PSI to PEDOT:PSS ratio, error bars represent standard deviations based on three measurements. The inset shows the near linearity of the data in the low PSI to PEDOT:PSS range.

(Supporting Information). The mixtures were sonicated for 10 min to improve dispersibility and allow for PSI−PEDOT:PSS interactions to replace PSI−TX-100 interactions. Generally, 500 μL of this solution was dropped onto a rotating, SAM-treated gold substrate (∼2 cm^2 in area) until solvent is completely evaporated. The substrate was rotated at speeds ranging from 500 to 4000 rpm for different times (∼1−2 min) to produce the composite film. A KW-4A spin coater purchased from Setcas LLC was used for all spin coating purposes.

Characterization. Infrared spectra were analyzed by attenuated total reflectance Fourier transform infrared (ATR-FTIR) spectroscopy using a Thermo Nicolet 6700 FT-IR spectrometer equipped with a liquid-nitrogen-cooled mercury−cadmium−telluride (MCT) detector and a Smart iTR ATR attachment with a diamond crystal plate. The spectra were collected in the region of 4000−700 cm^{-1} over 256 scans at 2 cm^{-1} resolution and processed using OMNIC software. The inherent diamond crystal in the FT-IR exposed to open air was used as the background for all data collection.

Scanning electron microscopy (SEM) images of PEDOT:PSS, 10 wt % PSI composite, and PSI films were taken using a Hitachi S-4200 SEM at an accelerating voltage of 2 kV. The PEDOT:PSS and 10 wt % PSI films were spin coated at 1250 rpm. The PSI film was drop casted and sputtered with gold for 20 s due to the insulating nature of the protein.

Profilometry was applied to study the roughness/uniformity of the produced films. Profilometric thickness was determined using a Veesco Dektak 150 stylus profilometer. Measurements were performed over 4000 μm using a stylus with a 12.5 μm radius, applying 2.0 mg force, and employing a hills-and-valleys detection mode.

Ellipsometric measurements were obtained on a JA Woollam Co. M-2000VI variable angle spectroscopic ellipsometer with WVASE32 software for modeling. Each sample was measured at two incident angles of 60° and 70° using a 632 nm HeNe laser. Film thickness was fitted from these measurements by using a B-spline fitting model atop a gold substrate.

Zeta sizing was used to determine the size distributions of PSI and PEDOT:PSS in the aqueous phase. A Malvern Panalytical Zeta Sizer Ultra was used to determine hydrodynamic diameters for different mixtures of particles in solution using multi-angle dynamic light scattering (MADLS). Measurements were taken at 25 °C with water as the dispersant. PSI was measured at a refractive index of 1.45 and an absorbance of 0.37, whereas PEDOT:PSS was measured at a refractive index of 1.40 and an absorbance of 0.90. To maintain similar concentrations and solution volumes, a PEDOT:PSS stock solution was diluted 80-fold prior to the MADLS analysis to a final concentration of 0.14 mg/mL, and 10 wt % PSI solution was diluted

50-fold for a final concentration of 0.14 mg/mL PEDOT:PSS and 0.014 mg/mL PSI.

An Ossila four-point probe system (product T2001A3-UK) was used to measure the conductive properties of films made on surface-treated glass. The measurements were recorded at 128 samples per point, a current of 1 μA, and a maximum voltage of 5 V. The applied current resulted in a total of 10 repeat values of sheet resistance, resistivity, and conductivity for each sample with the averages and standard deviations of three data sets as the reported results.

Photochronoamperometry (PCA) was performed using a three-electrode assembly and a CH660a potentiostat (CH Instruments, Austin, TX) equipped with a Faraday cage. Gold coated with the thin film served as the working electrode, Ag/AgCl was used as the reference electrode, and a platinum mesh served as the counter electrode. A cold light source (Leica KL 2500 LCD), which emitted a light intensity of 100 mW/cm^2 at a spectral range of 380−790 nm, was used during the 20 s light exposures. The photoelectrochemically active area during experiments was constrained to 0.27 cm^2. For the composite films, the open circuit potential (OCP) was first measured in the dark, and then the recorded value was applied to the film during the PCA data collection. Applying the OCP value quantified in the dark allows the background current to begin around zero, phasing out the inherent potential differential in the system and attributing any further change in current during the 20 s illumination period to reactions within the film and at the electrode surface. All PCA measurements were performed using a redox electrolyte containing 100 μM potassium hexacyanoferrate(II) trihydrate K$_4$[Fe(CN)$_6$]· 3H$_2$O, 100 μM potassium hexacyanoferrate(III) K$_3$[Fe(CN)$_6$], and 100 mM KCl.

■ RESULTS AND DISCUSSION

IR Spectroscopy. Prior to deposition, PSI and PEDOT:PSS were mixed to produce solutions with protein to polymer ratios ranging from 0.1 to 2.3 on a mass basis. Table S1 outlines the different weight percentages, ratios, and component concentrations of the resulting mixtures. PSI solutions were not dialyzed to remove TX-100 surfactant, and the mixtures of PSI and PEDOT:PSS were spin coated in the presence of TX-100 to produce uniform films. He et al. and Thomas et al. have previously shown that the spin coating of PEDOT:PSS is improved by mixing it with TX-100, which serves as a wetting agent to improve the wettability of the ICP on the substrate.[21,22] Here, spin coating in the absence of TX-100 hindered the mixing and produced films that were less uniform than those produced in its presence.

IR spectroscopy was used to determine the composition of the composite films produced by spin coating at a spin rate of 1500 rpm onto gold substrates prefunctionalized with a SAM prepared from AET. Figure 1a shows the IR spectra of the composite films and assigns key peaks to their molecular contributions. The different components present in the films (PSI, PEDOT:PSS, and TX-100) exhibit multiple peaks between 1000 and 1800 cm^{-1}. Composite films prepared at different ratios of PSI to PEDOT:PSS were observed to have different ratios of absorbances of key peaks.

The top spectrum of Figure 1a is a result of a drop casted film from a solution of PSI and TX-100. Drop casting was necessary to achieve a PSI control here because spin coating of the pure protein results in a very thin film that yields poor signal-to-noise in the IR spectrum. The presence of PSI in the drop casted film is consistent with the observation of Amide I and II peaks representing protein C═O and N−H/C−N vibrational modes at ∼1660 and 1552 cm^{-1}, respectively.[23−25] TX-100 is present in the PSI film as a broad peak centered around 1110 cm^{-1} which is assigned to the antisymmetric vibrational mode of the C−O−C group.[26] The bottom IR

spectrum in Figure 1a is spin coated PEDOT:PSS. The presence of PSS in that film is consistent with two peaks relating to S═O stretching of sulfonate bonds at around 1010 and 1040 cm^{-1}. PEDOT is evident from the inter-ring stretching at 1526 cm^{-1} and from the C−C or C═C quinoidal structure of thiophene at 1328 cm^{-1}.[27,28] Figure S2 helps to identify PEDOT from PSS peaks where IR spectra of both sodium PSS and PEDOT:PSS are plotted on the same scale. The peak at 1416 cm^{-1} is believed to be a combination resulting from PEDOT and PSS and is attributed to CH$_2$ bonds of a cyclic structure that are near an oxygen atom.[29]

For the other three spectra at solution ratios of 0.010, 0.11, and 0.25 PSI to PEDOT:PSS, we trace characteristic absorbances for both PSI and PEDOT:PSS, supporting the presence of these two components in the resulting film. The relative absorbance of the Amide I band of PSI at 1660 cm^{-1} increases relative to those attributed to PEDOT:PSS as the solution-phase ratio increases. The presence of TX-100, however, is less apparent in the film, as most of it spins off during the deposition process. Because PEDOT:PSS contains both negative and positive surface charges as well as hydrophobic patches that could interact well with the charged regions and hydrophobic belt of PSI, respectively, the polymer likely exchanges with the surfactant to replace its interactions with the protein during the process of liquid mixing and sonication, rendering the latter mostly unbound and easy to spin off the surface with the unretained aqueous phase. Apparently, TX-100 exhibits weaker attractions toward the PSI protein than does PEDOT:PSS. This result illustrates the favorable interactions between the polymer and the protein, which allows for bypassing of the dialysis process for PSI deposition. Figure 1a then confirms the presence of spin coated material in the film, that the change of compositions in the liquid phase are fairly translated to the solid phase, and that favorable interactions are present between PSI and PEDOT:PSS.

To quantify how the PSI to PEDOT:PSS ratio in the spin coated films trends with that in solution, an FTIR/ATR peak analysis was used to compare the different characteristic peaks for these solutions made at different compositions. Figure 1b is a plot of the ratios of areas of the Amide I peak for PSI at 1660 cm^{-1} to three different peaks, namely, those for the CH$_2$ bonds in the cyclic structures near an oxygen atom peak for PEDOT:PSS at 1416 cm^{-1}, the PSS S═O stretching of sulfonate bonds at around 1010 cm^{-1}, and the PEDOT inter-ring stretching at 1526 cm^{-1}. Figure 1b reflects a positive correlation between the amount of PSI in solution and its IR absorbance within the film. At low PSI to PEDOT:PSS ratios (up to 0.11), we observe a nearly linear trend in accordance with Beer−Lambert's law stating that absorbance scales linearly with material concentration. The proportion factors between the three data points at a given concentration in the dilute PSI system are constant, meaning that there is no specific enrichment or depletion of PEDOT, PSS, or PSI within the film at the 0.01 to 0.11 PSI to PEDOT:PSS range and that the concentration of PSI is increasing proportionally in the film relative to the solution-phase concentrations. At higher protein-to-polymer ratios, the peak ratios increase nonlinearly, indicating that PSI is preferentially retained within the film, which is consistent with the presence of larger protein aggregates. At lower PSI concentrations, the film mainly consists of a large network of intertwined polymer chains that are sufficiently abundant to interact more favorably with and

stabilize individual PSI proteins that no longer require the stabilization by TX-100. As the concentration of PEDOT:PSS decreases, the protein favors its own intermolecular interactions over the ones provided by PEDOT:PSS, creating multimolecular structures that agglomerate in the absence of TX-100. These multiprotein structures likely become entrapped within the PEDOT:PSS matrix rather than the larger matrix stabilizing single proteins, subsequently increasing the final concentration of the protein in the film and allowing the aggregates to be entrapped in the solid state.

SEM Imaging. We used SEM to characterize the morphology of a PEDOT:PSS film, a 10 wt % PSI composite film, and a pure PSI film as shown in Figures 2a, 2b, and 2c, respectively. Spin coating pristine PEDOT:PSS results in
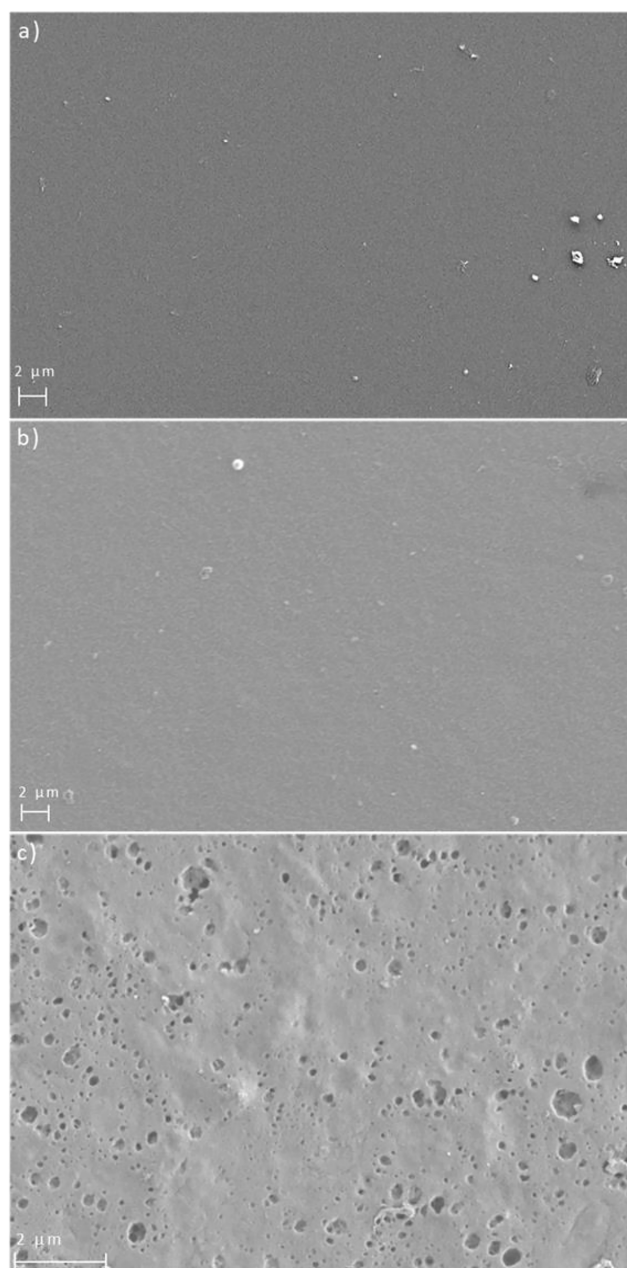

Figure 2. SEM images of (a) pristine PEDOT:PSS, (b) 10 wt % PSI, and (c) pristine PSI films. The morphology of the 10 wt % PSI film more closely resembles that of pristine PEDOT:PSS.

uniform films with little to no features in the surface morphology (Figure 2a). PSI alone yields a much different film (Figure 2c) than that of the polymer, with the SEM image showing a porous film across the entire scanned distance. When mixed at 10 wt % PSI, the resulting composite film exhibits a morphology that most closely resembles that of pristine PEDOT:PSS (Figure 2b). This composite film is thus mostly PEDOT:PSS with PSI proteins entrapped within the polymer matrix. Figure 2b shows no indications of a phase-separated system and provides further support that PSI and PEDOT:PSS are well-mixed at 10 wt % PSI.

Profilometry. Profilometry was applied to study the thickness and uniformity of the polymer−protein hybrid films and compare two deposition techniques: drop casting and spin coating. Figure 3a represents profilometry measurements across 1.5 mm of both films that are 10 wt % PSI. The PSI-containing solution was diluted 10-fold in DI water prior to the drop casting process to obtain a film with thickness on a similar scale as that for the film deposited via spin coating. For the drop casting, an electrochemical mask was used to maintain the liquid solution, and the water was removed by evaporation for ∼1 h to obtain the desired solid film.

Spin coating yields a film with a controllable thickness of ∼250 nm produced at 1250 rpm that is more uniform than that from drop casting. A uniform film is advantageous in most applications, including photoelectrochemical cells and devices. As shown in Figure 3a, the drop casted film exhibits the classic coffee-ring effect where the edges of the film are much thicker than is its center. Also, the spin coated film was fabricated in only 1 min, as compared to 1 h for the drop casted film, cutting the deposition time by 60-fold. In addition, spin coating avoids the use of a hydrophobic mask that sometimes limits the surface area of the deposited film and exacerbates the coffee-ring effect. Lastly, films produced by spin coating are much thinner (generally 100−300 nm) than the drop casted films, which can exceed 1000 nm. Thus, a key drawback of the lower roughness and superior uniformity is that spin coating results in a thinner film with a much greater loss of material. For spin coating, ∼130 μL/cm^2 of the initial, concentrated 0.11 PSI to PEDOT:PSS solution is dispensed, whereas only ∼19 μL/cm^2 of that solution is used for drop casting. Typical spin coating processes utilize only 2%−5% of the material dispensed onto the substrate while the remaining 95%−98% is spun off into the spin coater bowl and lost as waste.[30] Given the ease of extraction and vast abundance of PSI and the low cost of the PEDOT:PSS, this disadvantage is far from detrimental.

A key feature of spin coating is the ability to adjust the film thickness by simply changing the spin speed. Fine tuning the thickness of the resulting thin films is paramount because the thickness dictates the total loading of the PSI and PEDOT:PSS components. Here, we emphasize how spin coating can drastically change the thickness of the film by controlling a single parameter, the spin speed, a simple tuning ability that most other deposition methods do not offer. Figure 3b shows how slight modifications in the spin speed can greatly affect the thickness of the film, and it also highlights the ability to obtain more uniform films than in drop casting (Figure 3a), which would enable the resulting photoelectrochemical device to operate more predictably. For this sample at 10 wt % PSI in the solution solute, we obtain an average roughness of about 10 nm and spatially consistent films over the entire linear scan. By equating centrifugal forces to viscous forces in the cylindrical radial momentum equation for flow of viscous
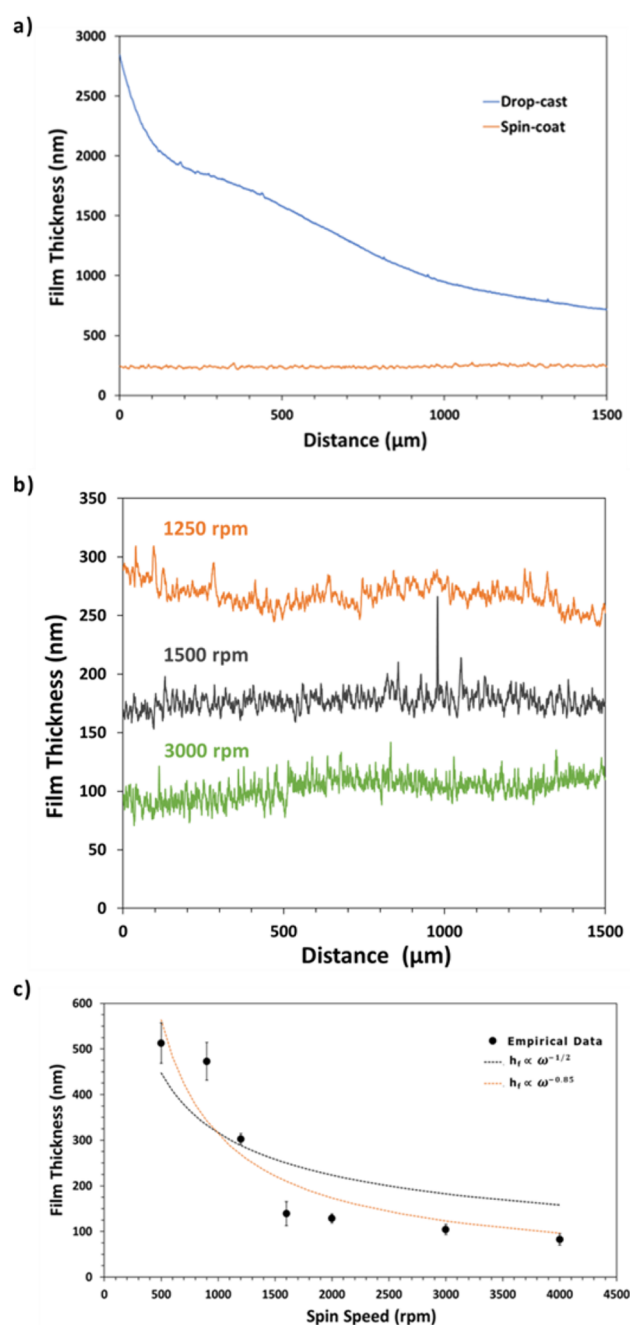
Figure 3. (a) Profiles representing the thickness of the deposited layer from a 10 wt % PSI solution via spin coating or drop casting with the scanned distance starting near the edges of the films. The same solution was diluted 10-fold prior to drop casting. (b) Profiles of composite PSI−PEDOT:PSS films at 10 wt % PSI in solution, where film thickness is inversely correlated to spin speed. (c) Average film thickness at different speeds for various composite films made at 10 wt % PSI. The black dotted line in which thickness varies as $\omega^{-1/2}$ is the result of the analysis of transport phenomena in a spin coating process, while the orange dotted line corresponding to a dependence of $\omega^{-0.85}$ is the best fit model for all data points. Error bars show the expected range for the average film thickness over the spread of the scanned distance.

liquid on a rotating disk, we can estimate the expected thickness of a spin coated film. Based on equations derived by Meyerhofer,[31] assuming that the liquid of interest behaves as a Newtonian fluid, shear resistance is applicable only in the horizontal direction, and spin-off is dominant over solvent evaporation, the expected thickness of a spin coated film is

$$h_{\mathrm{f}} = \frac{C_0}{\sqrt{\omega}} \left[\frac{3k\nu_0}{2(1 - C_0)} \right]^{1/3} \tag{1}$$
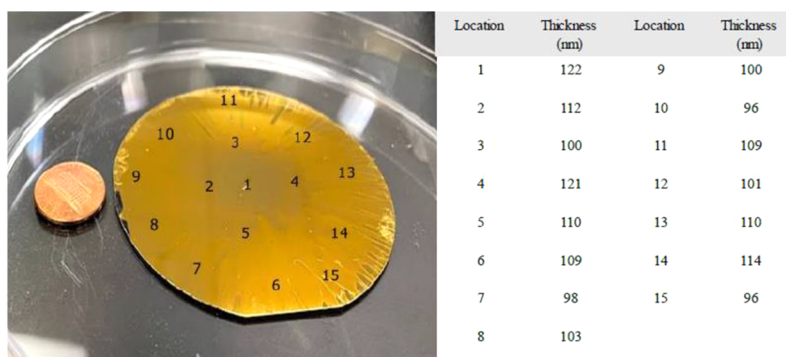
where C_0 is the initial concentration of solute, k is a constant specific to the coating solvent, ω is the angular velocity, and ν_0 is the kinematic viscosity of the solution dispensed. The general correlation predicts that the final film thickness (h_{f}) of a film is proportional to $\frac{1}{\sqrt{\omega}}$, meaning that a film spun at a speed 4 times greater than its counterpart would be half as thick. Profilometry was used to measure the thickness and uniformity of the produced films, which exhibit roughness on the order of ∼10 nm. Figure 3c shows the effect of spin speed on the average profilometric thickness of films made at 10 wt % PSI in solution for a scanned distance of 4 mm. The film thickness diminishes from an average of 513 nm at 500 rpm to an average value of 83 nm at 4000 rpm. The collected data are compared to the predictive model in eq 1 where a proportionality factor (C) accounts for all parameters other than spin speed and is solved by using MATLAB's curve fitting tool. The predicted correlation follows the general trend of the actual measured thickness, but its accuracy is limited by the fact that the thicknesses of the resulting films depend on parameters such as solvent viscosity, vapor pressure, temperature, and local humidity that are not accounted for in eq 1.[32] To obtain a better fit of the data, another model was employed where both the proportionality constant (C_1) and the power of the angular velocity (x) are determined as

$$h_{\mathrm{f}} = C_1 \omega^x \tag{2}$$

For the best fit model, we found that film thickness scales best with $\omega^{-0.85}$, demonstrating a higher negative dependence of film thickness on spin speed than eq 1 predicts. The stronger negative dependence on spin speed is not likely due to non-Newtonian effects because the fabricated films are uniform.[33] Such a higher negative dependence on spin speed up to −1 occurs for systems with limited evaporative effects.[34] Solvent-evaporation effects are known to have a significant impact on the final thickness of a spin coated film.[35] The solvent being used, in this case water, is less volatile than most organic solvents that are commonly used in spin coating. Thus, the empirical data are best fitted to the $\omega^{-0.85}$ model, reinforcing the negative relationship between spin speed and film thickness.

Given that different applications require different film thicknesses, we explored multistep spin coating of composite films atop each other at a speed of 1500 rpm. We observed that achieving more than two continuous and rapid depositions via spin coating poses a challenge but allowing the film to air-dry for a few minutes between depositions grants a successful layering of four depositions as shown in Figure S3. The thickness increases in a nearly linear fashion with each deposition step and, for the system and speed specified, increases from ∼100 nm to a final thickness of ∼400 nm, indicating another tunable element of the spin coating deposition technique.

Substrate Scale-Up. Spin coating was also explored for large substrate accommodation and scalability. We were able to successfully spin coat the composite film on a ∼44 cm² wafer,

Location	Thickness (nm)	Location	Thickness (nm)
1	122	9	100
2	112	10	96
3	100	11	109
4	121	12	101
5	110	13	110
6	109	14	114
7	98	15	96
8	103		

Figure 4. A composite film made from 10 wt % PSI in solution on an ~44 cm^2 gold substrate at 1500 rpm spin speed and the corresponding thicknesses measured at different locations of the film. A penny is used for scale.
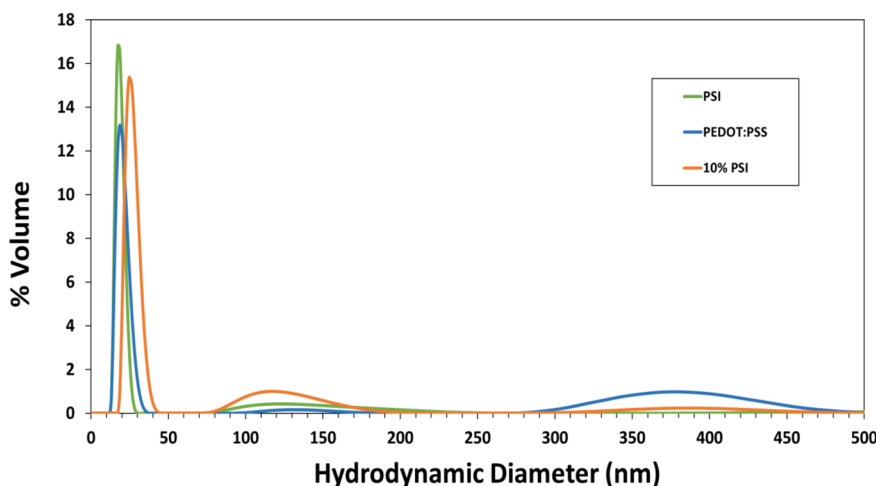
Figure 5. Size distribution by % volume of PSI, PEDOT:PSS, and a 10% PSI solution showing the hydrodynamic diameter of the particles.

enabling larger scale deposition of these composite films. Figure 4 shows the resulting large wafer that is covered by the PSI−PEDOT:PSS coating where 2 mL of the 10 wt % PSI (in solute) solution was dispensed over the AET/Au substrate at 1500 rpm. Ellipsometric measurements at 15 different locations on the sample, where streaking is not prominent as it is in some areas toward the edges, all indicate values of ~100 nm for the film, with the average over the entire measured area being 107 nm with a standard deviation of only 8 nm. Thus, large-scale (substrate area >25 cm^2) PSI−PEDOT:PSS composite films of the order of hundreds of nanometers can be quickly and easily produced while retaining photoactivity of the protein.

Polymer−Protein Size Distributions and Interfacial Interactions. To better understand the interactions present in the protein−polymer solution that is being spin coated, we investigated the size distribution of each component, as well as a 10 wt % PSI mixture, using multi-angle dynamic light scattering (MADLS). The size distribution of PSI will depend on the extraction procedure, namely, what surfactant is being used, as different surfactants (for example, ionic vs nonionic) based on their charge and size have an effect on the protein's size in solution.[36] The size of the polymer will depend more on the procedure in which it was synthesized, which affects its molecular weight, conductivity grade, and concentration in solution,[37] with Namkoong et al. reporting PEDOT:PSS having a nanoscale size smaller than 100 nm.[38] Boekema et

al. looked at the crystal structure of PSI from spinach identifying its dimensions to 16 × 12 nm^2.[39] TX-100 alone has been reported to have a radius of gyration ~4 nm while forming micelles that vary from 4 to 7 nm in size depending on its concentration in solution. Thus, PSI stabilized by TX-100 surfactant is expected to have a size distribution that is a combination of both components.[40,41] Based on published procedures and to exclude any large aggregates or impurities from distorting the size data, the PEDOT:PSS stock solution was filtered with a 0.45 μm cellulose filter, and extracted PSI solutions were filtered with a 0.22 μm cellulose filter. MADLS results are shown in Figure 5 where PSI, with the TX-100 surfactant shell, mainly exhibited a hydrodynamic diameter (d_h) size distribution centered at ~19 nm with its resulting curve reflecting a narrow distribution around that value with some larger trace aggregates around 125 nm. Filtered PEDOT:PSS is more polydisperse as it exhibits multiple peaks in its size distribution. PEDOT:PSS is found to be mostly present at ~22 nm, but also at sizes centered around 125 and 370 nm. In these polydisperse solutions, larger particles scatter more light, as shown in Figure S4.

The polydisperse size distribution for the combination of 10% PSI reflects a mixed system where PSI and PEDOT:PSS achieve favorable interactions. When PSI and PEDOT:PSS are mixed, the primary peak for 10 wt % PSI shifts to a higher d_h than that of PSI alone, appearing at ~25 nm in Figure 5. This larger hydrodynamic radius is not consistent with two distinct

populations of PSI+TX-100 and PEDOT:PSS. In this mixture, TX-100 interactions are greatly depleted as indicated by the IR spectra of the films in Figure 1a. The resulting favorable PSI−PEDOT:PSS interactions are attributed to some of the flexible chains of the polymer electrostatically stabilizing the protein. The stabilizing interactions are sufficient to enable successful spin coating of a membrane protein in a thin film, while ridding it of its surfactant.

Film Conductivity Measured Using a Four-Point Probe. A four-point probe was used to measure conductivity values of films of PSI−PEDOT:PSS spin coated at different compositions on silane-functionalized glass. The conductivity of the composite film is highly dependent on the conductivity of PEDOT:PSS, the only conducting component in these films. We purchased a high conductivity grade of PEDOT:PSS to overcome the inherent bulky and resistive nature of the protein that would tend to hinder the movement of electrons within the film. Table 1 shows the conductivities and resistances of films tested right after deposition and compares results with those that were treated in a vacuum oven at 50 °C for 1 h.

Table 1. Conductivity of Films Spin Coated on Silane-Treated Glass at Different PSI−PEDOT:PSS Loadings in Solution, with and without Heating at 50 °C for 1 h

PSI to PEDOT:PSS ratio	conductivity (S/m)	
	as cast	annealed
0	1.8 ± 0.1	2.5 ± 0.2
0.010	1.1 ± 0.2	2.0 ± 0.1
0.053	0.43 ± 0.02	0.87 ± 0.05
0.11	0.20 ± 0.01	0.43 ± 0.09
PSI only	0	0

All films containing the two components at the ratios prepared reveal conductive behavior. As expected, PSI alone is not conductive. Exposing the protein−polymer mixture to mild temperatures that do not cause PSI denaturation allows for additional water to evaporate from the film, causing the conductivity to increase and the sheet resistance to decrease, but films were still conductive as deposited. The more PSI in the film, the less conductive the film becomes, so there is a trade-off between conductivity and photoactivity within these films. The conductivity for a ∼100 nm thin film drops from 2.5 to 0.4 S/m as the ratio of PSI to polymer is increased from 0 to 0.11. Even at a ratio of 0.01, there is an ∼20% and ∼40% decrease in conductivity from a pure PEDOT:PSS film with and without annealing, respectively, suggesting good mixing of the components in the film. If the two components were phase-separated within the film at such low protein loading, the conductivity is expected to be much closer to that of the more conductive component, PEDOT:PSS. For example, a phase-separated film at a ratio of 0.01 would have been expected to yield a conductivity that is ∼99% of the conductivity of pristine PEDOT:PSS, rather than the much lower observed conductivity.[42] Pal et al. made similar conclusions regarding mixing in composite films containing a sericin protein photoresist and PEDOT:PSS.[43] These conductivity results show that the composite film is conductive and support that PSI is well distributed in the film. The effect of annealing is also highlighted here, where nanostructural modifications in crystalline ordering, size expansion of PEDOT:PSS, and PSS chain rearrangements can all have an overall effect on improving the conductivity of the ICP.[44,45]

Photochronoamperometric (PCA) Measurements. PCA measurements were used to investigate the photo-electrochemical properties of the composite protein−polymer films and to understand their photoactive nature with respect to PSI loading. PCA measurements were performed in a solution of the ferricyanide ($Fe(CN)_6^{3-}$)/ferrocyanide (Fe-$(CN)_6^{4-}$) redox couple that has a redox potential of $E^{0'} = 0.2$ V vs Ag/AgCl, which is favorable to transfer electrons with PSI.[46] Figure 6a shows PCA curves for the PSI−PEDOT:PSS thin films initially in the dark for 20 s and then under a white light intensity of 100 mW/cm^2. The film of pure PEDOT:PSS does not exhibit a photocurrent, but all films containing PSI show significant photocurrents with the highest peak density of ∼0.7 μA/cm^2 for the film with the ratio of 0.11 PSI to PEDOT:PSS. To normalize the current density to the level of each protein in the film on average, the turnover number $\left(\frac{mol_{e^-}}{s \cdot mol_{PSI}}\right)$ was calculated (eq 3)

$$TN = \frac{i_{PCA}}{C_{PSI}F} \tag{3}$$

where i_{PCA} $\left(\frac{A}{cm^2}\right)$ is the pseudo-steady state current measured from the PCA runs, C_{PSI} $\left(\frac{mol_{PSI}}{cm^2}\right)$ is the areal concentration of PSI in the solid film (sample calculations shown in the Supporting Information), and F $\left(\frac{C}{mol_{e^-}}\right)$ is Faraday's constant. Increases in TN reflect more efficient utilization of the proteins within a given system. Figure 6b displays turnover numbers at different PSI loadings with sample calculations shown for drop casted and spin coated films in the Supporting Information. The highest turnover number is 4.8 e$^-$/s for the 1 wt % PSI film, which is the most dilute PSI film prepared. After entrapping PSI within the conducting polymer polyaniline in a solid-state system, Gizzie et al.[47] showed large effects on photocurrent at dilute PSI concentrations, suggesting that a high ratio of polymer to protein achieves effective interfacial areas for direct electron transfer (DET). Moreover, Figure 6b shows that the PSI−PEDOT:PSS composite films exhibit dramatically higher TNs than that of pure PSI (9.8×10^{-3} mol$_{e^-}$/s·mol$_{PSI}$), even though PEDOT:PSS alone does not exhibit any photoactivity. The TN also decreases with increased PSI loading, reflecting the lower conductivity of the composite film when the concentration of PSI increases within the film (Table 1). This increase in PSI loading occurs concurrently with more PSI−PSI interactions and thereby fewer interactions of individual proteins with polymer, following the same trend as PSI enrichment within the film (Figure 1b) at higher protein-to-polymer ratios. The enhancement of TN at low PSI loading suggests that DET occurs in the system, with the mechanism shown in Figure 6c to explain the observed anodic current in Figure 6a. Here, the gold substrate is held at the OCP of ∼+0.2 V vs Ag/AgCl (∼+0.4 V vs NHE) measured in the dark, pushing electrons from the redox mediators toward the working electrode (WE). PEDOT:PSS behaves as a semiconductor, receiving the photoexcited electrons from PSI through its conduction band and channeling these electrons toward the WE. Thus, the PCA results shown here further reinforce the presence of strong PSI/PEDOT:PSS interactions that support DET in the composite film.
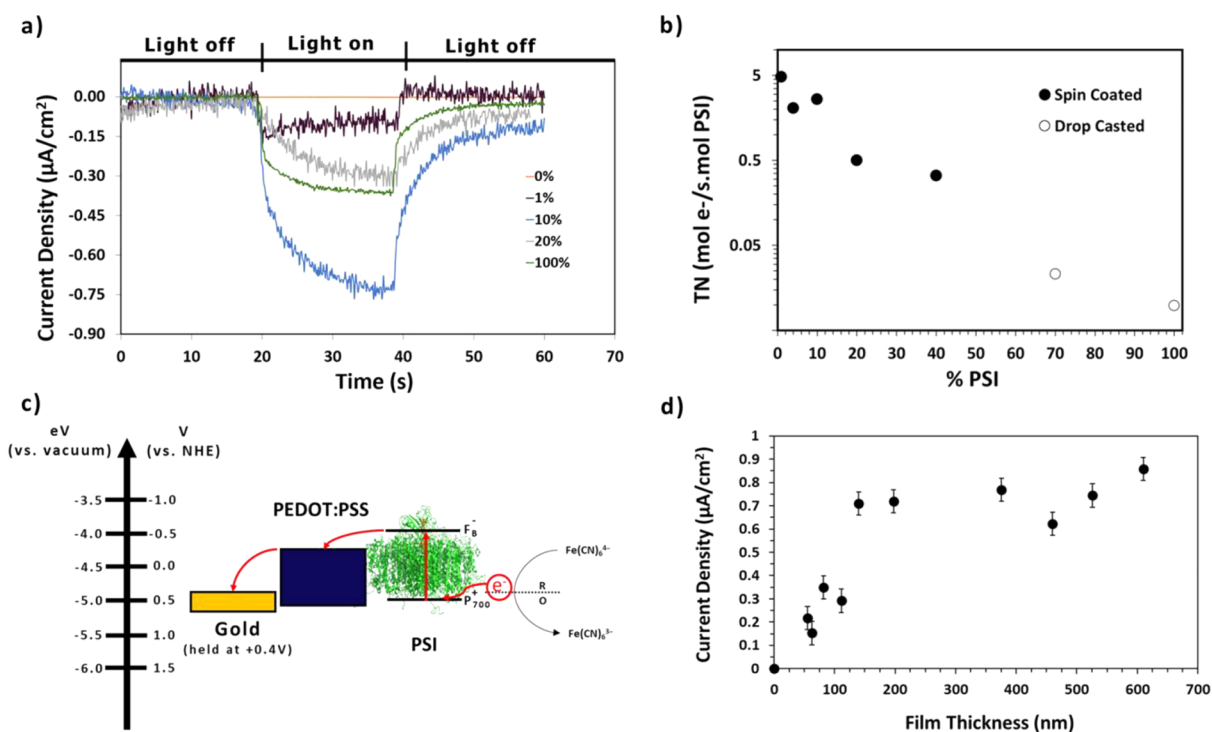
Figure 6. (a) PCA measurements of films of similar thicknesses of ∼150 nm, but with different PSI and PEDOT:PSS loadings, measured in ferricyanide $(Fe(CN)_6{}^{3-})$/ferrocyanide $(Fe(CN)_6{}^{4-})$ mediator solutions. The legend represents the wt % of PSI in solution. (b) Semilog plot of the turnover number for the PCA measurements from (a) along with additional data points for spin coated (1−40% PSI) and drop casted (70−100% PSI) films. (c) Schematic of the proposed electron transfer mechanism between the redox mediator, the composite film, and the gold substrate, neglecting recombination effects that are more likely to dominate at greater film thicknesses. (d) Steady-state current density of films made from 0.11 PSI to PEDOT:PSS solutions at different thicknesses (by varying spin speed) and measured in ferricyanide $(Fe(CN)_6{}^{3-})$/ferrocyanide $(Fe(CN)_6{}^{4-})$ mediator solutions. Error bars represent the inherent standard error in PCA measurements.

The effect of film thickness on photocurrent for a given PSI to PEDOT:PSS ratio was investigated to better understand the electrode/active layer interface. Composite films at 0.11 PSI to PEDOT:PSS, given their high photoactivity and reproducibility, were deposited on gold substrates at different thicknesses by altering spin speed and volume dispensed in the spin coating process. Figure 6d shows that the photocurrent density increases with thickness until it reaches an asymptotic value of ∼0.7 $\mu A/cm^2$ at thicknesses nearing and greater than ∼140 nm. Such a limiting thickness could be related to restricted light penetration due to the high optical density and opaque nature of PEDOT:PSS stock solution or charge recombination. However, UV−vis data in Figure S5 show that light passes through the entirety of a 10% PSI composite film that is ∼865 nm thick with recorded % transmittance as high as 46% and 65% for the two chlorophyll *a* characteristic peaks at 675 and 440 nm, respectively. Thus, light penetration is not a limiting factor for the photoactivity of the composite films. Therefore, charge recombination is a more probable scenario in limiting photocurrents of thicker films. Given the mechanism proposed in Figure 6c, the oxidized mediator $(Fe(CN)_6{}^{3-})$ or the oxidized PSI active site (P700+) could capture electrons routed from PSI through PEDOT:PSS, causing a hole−electron recombination effect. PEDOT:PSS has previously been shown to enhance current for ferricyanide/ferrocyanide redox reactions, suggesting the polymer's aptness to exchange electrons with the mediator.[48] For thicker films, the longer time scale and the greater distance through the composite film that photogenerated electrons must travel to reach the electrode allow a greater probability of

these recombination events to limit the current. For thinner films and for the bottom ∼140 nm of any film, this time scale for electron transfer is sufficiently fast that photocurrent increases with thickness. Therefore, an optimal thickness of ∼140 nm is recommended for highest photoactivity and minimal material usage for composite films fabricated from solutions with 10 wt % PSI and 90 wt % PEDOT:PSS in the solute.

■ CONCLUSION

PEDOT:PSS, an intrinsically conductive polymer, can be incorporated with PSI proteins in aqueous solution to enable the spin coating of uniform, conductive, and photoactive PSI−PEDOT:PSS composite films. The spin coated protein−polymer films are far more uniform as compared to films obtained by drop casting, although loss of components by spin-off is pronounced. The spin coating process can be easily tuned to generate these biohybrid composite films with different thicknesses on the order of hundreds of nanometers, and the process can be scaled up to at least ∼44 cm^2 to prepare uniform composite films over large areas. At low PSI loadings, MADLS, IR, four-point probe, and PCA all suggest favorable interactions between PSI and PEDOT:PSS at the molecular level, as the polymer replaces interactions between PSI and TX-100 to stabilize individual proteins in the composite film and to yield enhanced conductivities and photoelectrochemical currents. As a measure of efficient integration of PSI within the film, the TN is well above 1 e^-/s for 1, 5, and 10 wt % PSI but decreases at higher protein loadings. Higher PSI concen-

trations in solution resulted in a disproportionately higher enrichment of the protein within the composite films, consistent with protein aggregation and leading to less uniform films with lower photoelectrochemical performance. These results reveal the importance of high film conductivity and high interfacial area between individual proteins and ICP, which are both enhanced at low PSI loadings. We conclude that these scalable, conductive, and photoactive PEDOT:PSS−PSI composite films prepared by spin coating from aqueous solution show potential for the design and fabrication of photoelectrochemical devices.

■ ASSOCIATED CONTENT

ⓈⒾ Supporting Information

The Supporting Information is available free of charge at https://pubs.acs.org/doi/10.1021/acsapm.2c02126.

> Different weight percentages and ratios of PSI and PEDOT:PSS mixed in solution; profilometry of a spin coated pure PSI film; IR spectra of pristine PEDOT:PSS and sodium PSS; the varying thickness from 1 to 4 spin coated layers at 10 wt % PSI; turnover number sample calculations; MADLS percentage intensity data; UV−vis transmittance data for a film fabricated from 10 wt % PSI solution (PDF)

■ AUTHOR INFORMATION

Corresponding Author

G. Kane Jennings − *Department of Chemical and Biomolecular Engineering, Vanderbilt University, Nashville, Tennessee 37235-1604, United States;* ⓞ orcid.org/0000-0002-3531-7388; Email: kane.g.jennings@vanderbilt.edu

Authors

Marc A. Nabhan − *Department of Chemical and Biomolecular Engineering, Vanderbilt University, Nashville, Tennessee 37235-1604, United States;* ⓞ orcid.org/0000-0003-0106-9467

Carlos A. Silvera Batista − *Department of Chemical and Biomolecular Engineering, Vanderbilt University, Nashville, Tennessee 37235-1604, United States;* ⓞ orcid.org/0000-0002-3509-601X

David E. Cliffel − *Department of Chemistry, Vanderbilt University, Nashville, Tennessee 37235-1822, United States;* ⓞ orcid.org/0000-0001-8756-106X

Complete contact information is available at:
https://pubs.acs.org/10.1021/acsapm.2c02126

Notes

The authors declare no competing financial interest.

■ ACKNOWLEDGMENTS

■ ABBREVIATIONS

PSI, photosystem I; PEDOT:PSS, poly(3,4-ethylene-dioxythiophene):polystyrenesulfonate; ICP, intrinsically conducting polymer; SEM, scanning electron microscopy; TX-100, Triton X-100; FTIR, Fourier transform infrared spectroscopy; ATR, attenuated total reflectance; PCA, photochronoamperometric; TN, turnover number; OCP, open-circuit potential; LbL, layer-by-layer.

■ REFERENCES

(1) Fromme, P.; Mathis, P. Unraveling the Photosystem I Reaction Center: A History, or the Sum of Many Efforts. *Photosynthesis Research* **2004**, *80* (1−3), 109−124.

(2) Ciesielski, P. N.; Hijazi, F. M.; Scott, A. M.; Faulkner, C. J.; Beard, L.; Emmett, K.; Rosenthal, S. J.; Cliffel, D.; Jennings, G. K. Photosystem I - Based Biohybrid Photoelectrochemical Cells. *Bioresour. Technol.* **2010**, *101* (9), 3047−3053.

(3) Nelson, N.; Yocum, C. F. Structure and Function of Photosystems I and II. *Annual Review of Plant Biology* **2006**, *57*, 521−565.

(4) Kothe, T.; Pöller, S.; Zhao, F.; Fortgang, P.; Rögner, M.; Schuhmann, W.; Plumeré, N. Engineered Electron-Transfer Chain in Photosystem 1 Based Photocathodes Outperforms Electron-Transfer Rates in Natural Photosynthesis. *Chem. - A Eur. J.* **2014**, *20* (35), 11029−11034.

(5) Wolfe, K. D.; Dervishogullari, D.; Passantino, J. M.; Stachurski, C. D.; Jennings, G. K.; Cliffel, D. E. Improving the Stability of Photosystem I−Based Bioelectrodes for Solar Energy Conversion. *Curr. Opin. Electrochem.* **2020**, *19*, 27−34.

(6) Wang, Y. X.; Robertson, J. L.; Spillman, W. B., Jr.; Claus, R. O. Effects of the Chemical Structure and the Surface Properties of Polymeric Biomaterials on Their Biocompatibility. *Pharm. Res.* **2004**, *21* (8), 1362−1373.

(7) Yildirim, E.; Zhu, Q.; Wu, G.; Tan, T. L.; Xu, J.; Yang, S. W. Self-Organization of PEDOT:PSS Induced by Green and Water-Soluble Organic Molecules. *J. Phys. Chem. C* **2019**, *123* (15), 9745−9755.

(8) Yan, H.; Jo, T.; Okuzaki, H. Highly Conductive and Transparent Poly(3, 4-Ethylenedioxythiophene)/Poly(4- Styrenesulfonate) (PEDOT/PSS) Thin Films. *Polym. J.* **2009**, *41* (12), 1028−1029.

(9) Lang, U.; Muller, E.; Naujoks, N.; Dual, J. Microscopical Investigations of PEDOT:PSS Thin Films. *Adv. Funct. Mater.* **2009**, *19* (8), 1215−1220.

(10) Dervishogullari, D.; Gizzie, E. A.; Jennings, G. K.; Cliffel, D. E. Polyviologen as Electron Transport Material in Photosystem I-Based Biophotovoltaic Cells. *Langmuir* **2018**, *34* (51), 15658−15664.

(11) Lin, C. H.; Chen, K. T.; Ho, J. R.; Cheng, J. W. J.; Tsiang, R. C. C. PEDOT:PSS/Graphene Nanocomposite Hole-Injection Layer in Polymer Light-Emitting Diodes. *J. Nanotechnol.* **2012**, *2012*, 952−958.

(12) Liu, L.; Choi, S. Self-Sustainable, High-Power-Density Bio-Solar Cells for Lab-on-a-Chip Applications. *Lab Chip* **2017**, *17* (22), 3817−3825.

(13) Wolfe, K. D.; Gargye, A.; Mwambutsa, F.; Than, L.; Cliffel, D. E.; Jennings, G. K. Layer-by-Layer Assembly of Photosystem I and PEDOT:PSS Biohybrid Films for Photocurrent Generation. *Langmuir* **2021**, *37* (35), 10481−10489.

(14) Ciesielski, P. N.; Scott, A. M.; Faulkner, C. J.; Berron, B. J.; Cliffel, D. E.; Jennings, G. K. Functionalized Nanoporous Gold Leaf Electrode Films for the Immobilization of Photosystem I. *ACS Nano* **2008**, *2* (12), 2465−2472.

(15) Li, H.; Buesen, D.; Williams, R.; Henig, J.; Stapf, S.; Mukherjee, K.; Freier, E.; Lubitz, W.; Winkler, M.; Happe, T.; Plumeré, N. Preventing the Coffee-Ring Effect and Aggregate Sedimentation by: In Situ Gelation of Monodisperse Materials. *Chem. Sci.* **2018**, *9*, 7596−7605.

(16) Gordiichuk, P. I.; Wetzelaer, G. J. A. H.; Rimmerman, D.; Gruszka, A.; De Vries, J. W.; Saller, M.; Gautier, D. A.; Catarci, S.; Pesce, D.; Richter, S.; Blom, P. W. M.; Herrmann, A. Solid-State Biophotovoltaic Cells Containing Photosystem I. *Adv. Mater.* **2014**, *26* (28), 4863−4869.

(17) Kincaid, H. A.; Niedringhaus, T.; Ciobanu, M.; Cliffel, D. E.; Jennings, G. K. Entrapment of Photosystem I within Self-Assembled Films. *Langmuir* **2006**, *22* (19), 8114−8120.

(18) Tong, X.; Trivedi, A.; Jia, H.; Zhang, M.; Wang, P. Enzymic Thin Film Coatings for Bioactive Materials. *Biotechnol. Prog.* **2008**, *24* (3), 714−719.

(19) Kazemzadeh, S.; Riazi, G.; Ajeian, R. Novel Approach of Biophotovoltaic Solid State Solar Cells Based on a Multilayer of PS1 Complexes as an Active Layer. *ACS Sustain. Chem. Eng.* **2017**, *5* (11), 9836−9840.

(20) Deng, X.; Njoroge, I.; Jennings, G. K. Surface-Initiated Polymer/Ionic Liquid Gel Films. *J. Phys. Chem. C* **2018**, *122* (11), 6033−6040.

(21) He, L.; Jiang, C.; Wang, H.; Lai, D.; Rusli. High Efficiency Planar Si/Organic Heterojunction Hybrid Solar Cells. *Appl. Phys. Lett.* **2012**, *100* (7), 073503.

(22) Thomas, J. P.; Zhao, L.; Abd-Ellah, M.; Heinig, N. F.; Leung, K. T. Interfacial Micropore Defect Formation in PEDOT:PSS-Si Hybrid Solar Cells Probed by TOF-SIMS 3D Chemical Imaging. *Anal. Chem.* **2013**, *85* (14), 6840−6845.

(23) Arrondo, J. L. R.; Goñi, F. M. Structure and Dynamics of Membrane Proteins as Studied by Infrared Spectroscopy. *Prog. Biophys. Mol. Biol.* **1999**, *72* (4), 367−405.

(24) Seshadri, S.; Khurana, R.; Fink, A. L. Fourier Transform Infrared Spectroscopy in Analysis of Protein Deposits. *Methods Enzymol.* **1999**, *309*, 559−576.

(25) Ruan, X.; Wei, J.; Xu, Q.; Wang, J. S.; Gong, Y. D.; Zhang, X. F.; Kuang, T. Y.; Zhao, N. M. Comparison of the Effects of Triton X-100 Treatment on the Protein Secondary Structure of Photosystem I and Photosystem II Studied by FT-IR Spectroscopy. *J. Mol. Struct.* **2000**, *525* (1−3), 97−106.

(26) Greener, J.; Abbasi, B.; Kumacheva, E. Attenuated Total Reflection Fourier Transform Infrared Spectroscopy for On-Chip Monitoring of Solute Concentrations. *Lab Chip* **2010**, *10* (12), 1561−1566.

(27) Robinson, M. T.; Simons, C. E.; Cliffel, D. E.; Jennings, G. K. Photocatalytic Photosystem I/PEDOT Composite Films Prepared by Vapor-Phase Polymerization. *Nanoscale* **2017**, *9* (18), 6158−6166.

(28) Zhang, X.; Chang, D.; Liu, J.; Luo, Y. Conducting Polymer Aerogels from Supercritical CO_2 Drying PEDOT-PSS Hydrogels. *J. Mater. Chem.* **2010**, *20* (24), 5080−5085.

(29) Socrates, G. *Infrared and Raman Characteristic Group Frequencies: Tables and Charts*, 3rd ed.; J. Wiley and Sons: Chichester, UK, 2001.

(30) Mandoj, F.; Nardis, S.; Di Natale, C.; Paolesse, R. Porphyrinoid Thin Films for Chemical Sensing. *Encyclopedia of Interfacial Chemistry: Surface Science and Electrochemistry* **2018**, 422−443.

(31) Meyerhofer, D. Characteristics of Resist Films Produced by Spinning. *J. Appl. Phys.* **1978**, *49* (7), 3993.

(32) Emslie, A. G.; Bonner, F. T.; Peck, L. G. Flow of a Viscous Liquid on a Rotating Disk. *J. Appl. Phys.* **1958**, *29* (5), 858.

(33) Sukanek, P. C. Dependence of Film Thickness on Speed in Spin Coating. *J. Electrochem. Soc.* **1991**, *138* (6), 1712−1719.

(34) Britten, J. A.; Thomas, I. M. Non-Newtonian Flow Effects during Spin Coating Large-Area Optical Coatings with Colloidal Suspensions. *J. Appl. Phys.* **1992**, *71* (2), 972−979.

(35) Chen, B. T. Investigation of the Solvent-Evaporation Effect on Spin Coating of Thin Films. *Polymer Engineering and Science* **1983**, *23* (7), 399−403.

(36) Gunning, P. A.; MacKie, A. R.; Gunning, A. P.; Wilde, P. J.; Woodward, N. C.; Morris, V. J. The Effect of Surfactant Type on Protein Displacement from the Air-Water Interface. *Food Hydrocoll.* **2004**, *18* (3), 509−515.

(37) Abdou, M. S. A.; Lu, X.; Xie, Z. W.; Orfino, F.; Deen, M. J.; Holdcroft, S. Nature of Impurities in Pi-Conjugated Polymers Prepared by Ferric Chloride and Their Effect on the Electrical Properties of Metal-Insulator-Semiconductor Structures. *Chem. Mater.* **1995**, *7* (4), 631−641.

(38) Namkoong, G.; Younes, E. M.; Abdel-Fattah, T. M.; El-Maghraby, E. M.; Elsayed, A. H.; Abo Elazm, A. H. Aging Process of PEDOT:PSS Dispersion and Robust Recovery of Aged PEDOT:PSS as a Hole Transport Layer for Organic Solar Cells. *Org. Electron.* **2015**, *25*, 237−244.

(39) Boekema, E. J.; Boonstra, A. F.; Dekker, J. P.; Riigner, M. Electron Microscopic Structural Analysis of Photosystem I, Photosystem II, and the Cytochrome B6/f Complex from Green Plants and Cyanobacteria. *J. Bioenerg Biomembr.* **1994**, *26* (1), 17−29.

(40) Paradies, H. H. Shape and Size of a Nonionic Surfactant Micelle. Triton X-100 in Aqueous Solution. *J. Phys. Chem.* **1980**, *84* (6), 599−607.

(41) Denkova, P. S.; Lokeren, L. V.; Verbruggen, I.; Willem, R. Self-Aggregation and Supramolecular Structure Investigations of Triton X-100 and SDP2S by NOESY and Diffusion Ordered NMR Spectroscopy. *J. Phys. Chem. B* **2008**, *112* (35), 10935−10941.

(42) Ayub, A. N.; Ismail, N. A.; Aizamddin, M. F.; Bonnia, N. N.; Sulaiman, N. S.; Nadzri, N. I. M.; Mahat, M. M. Effects of Organic Solvent Doping on the Structural and Conductivity Properties of PEDOT: PSS Fabric. *J. Phys. Conf. Ser.* **2022**, *2169* (1), 012008.

(43) Pal, R. K.; Farghaly, A. A.; Wang, C.; Collinson, M. M.; Kundu, S. C.; Yadavalli, V. K. Conducting Polymer-Silk Biocomposites for Flexible and Biodegradable Electrochemical Sensors. *Biosens. Bioelectron.* **2016**, *81*, 294−302.

(44) Thomas, J. P.; Zhao, L.; McGillivray, D.; Leung, K. T. High-Efficiency Hybrid Solar Cells by Nanostructural Modification in PEDOT:PSS with Co-Solvent Addition. *J. Mater. Chem. A* **2014**, *2* (7), 2383−2389.

(45) Huang, J.; Miller, P. F.; De Mello, J. C.; De Mello, A. J.; Bradley, D. D. C. Influence of Thermal Treatment on the Conductivity and Morphology of PEDOT/PSS Films. *Synth. Met.* **2003**, *139* (3), 569−572.

(46) Chen, G.; LeBlanc, G.; Jennings, G. K.; Cliffel, D. E. Effect of Redox Mediator on the Photo-Induced Current of a Photosystem I Modified Electrode. *J. Electrochem. Soc.* **2013**, *160* (6), H315−H320.

(47) Gizzie, E. A.; Leblanc, G.; Jennings, G. K.; Cliffel, D. E. Electrochemical Preparation of Photosystem I-Polyaniline Composite Films for Biohybrid Solar Energy Conversion. *ACS Appl. Mater. Interfaces.* **2015**, *7* (18), 9328−9335.

(48) Benoudjit, A.; Bader, M. M.; Wan Salim, W. W. A. Study of Electropolymerized PEDOT:PSS Transducers for Application as Electrochemical Sensors in Aqueous Media. *Sens. Bio-Sensing Res.* **2018**, *17*, 18−24.